2.L

*Nuclear Physics* **A155** (1970) 89—108; © *North-Holland Publishing Co., Amsterdam*


# 166 MeV ELASTIC AND INELASTIC ALPHA-PARTICLE SCATTERING; MACROSCOPIC AND MICROSCOPIC ANALYSIS

B. TATISCHEFF and I. BRISSAUD

*Institut de Physique Nucléaire - B.P. no. 1, 91, Orsay, France*

Received 2 February 1970

(Revised 4 May 1970)

**Abstract:** Alpha-particle elastic scattering on $^{12}C$, $^{28}Si$, Sn, Pb and $^{2}H$ has been studied in order to obtain optical potential parameters. For each nucleus we find only one potential that gives a good fit, the situation being rather different from that existing at smaller energies. The first $2^+$ levels of C, Si and Sn and the first $3^-$ level of C were observed and the angular distribution of scattered α-particles analysed using the DWBA. Comparison has been made between theoretical and experimental deformation parameters. Optical potentials were calculated with an effective αN interaction and a matter distribution of the Fermi, shell-model or Hartree-Fock type. The agreement with elastic scattering results is very good. Differential cross sections for inelastic scattering obtained using these optical potentials and the same effective αN interaction in the DWBA matrix elements are compared with the experimental ones.

E

NUCLEAR REACTIONS $^{12}C$, $^{28}Si$, Sn, Pb, D(α, α) and (α, α'), $E_\alpha = 166$ MeV; measured $\sigma(E_\alpha, \theta)$; deduced optical-model parameters. $^{12}C$, $^{28}Si$, Sn levels deduced deformation parameters $\beta_l$. Enriched and natural targets. Optical potentials and deformation parameters deduced. αN interaction deduced.

## 1. Introduction

Alpha-particle elastic scattering has been investigated previously at small energies, chiefly below 45 MeV, and recently at 65 MeV [refs. [1,2])], 119 MeV [ref. [3])] and 104 MeV [ref. [4])]. Analysis has been made by several classical methods, but the most popular method is to use a complex optical potential of Woods-Saxon shape. Generally several alternative sets of parameters are found which will fit the data. This lack of uniqueness is believed to reflect the fact that the data determine only the value of the potential at the nuclear surface, leaving considerable ambiguity in the interior. However the interior region may act in some transfer or inelastic scattering reactions and the ambiguity of the potential in this region may change the predictions of DWBA calculations for these other reactions.

At higher energies, the strength of the αN interaction is decreasing. It is reasonable to think that the optical potential would be defined more deeply into the nucleus. For this reason we have measured the angular distribution of 166 MeV α-particles elastically scattered by several nuclei [5]). Our results may be interpreted using two different methods. First is the phenomenological Woods-Saxon potential or macroscopic analysis; here it is interesting to compare the parameters with those obtained at smaller

energies in order to examine their variation with energy up to 166 MeV. Second is a microscopic analysis [37]), the potential being calculated from a matter distribution and an effective αN interaction. Several questions arise with this method:

(i) Is it possible to obtain an effective αN interaction giving good results at different energies?

(ii) Is it possible to compare different matter distributions by means of such calculations?

We have also measured inelastic differential cross sections. For each excited level having a collective character, deformation parameters can be extracted using the macroscopic DWBA analysis. The distribution of the values obtained, for the same level but with different incident particles, will determine the interest – or the limitations of this method. Microscopic calculations can also be done using hole-particle (for

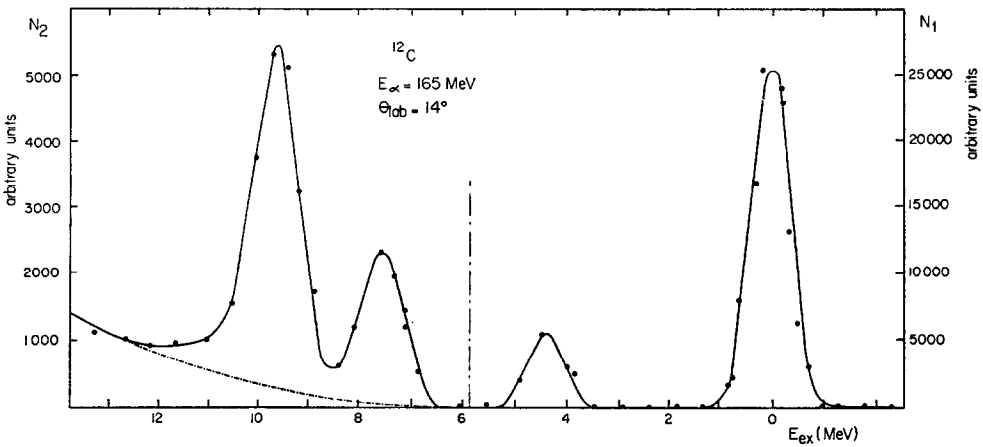


Fig. 1. Typical experimental spectrum showing the energy resolution.

carbon) or quasiparticle (for tin) wave functions and the same αN interaction as was used for elastic scattering.

The last question we want to discuss is the possibility of distinguishing between several proposed wave functions of excited levels, the best ones giving the best agreement with the experimental results. The interest of this study is that the calculations are done without any adjustable parameter.

## 2. Experimental lay-out

The beam from the ORSAY synchrocyclotron was used. The α-particle energy was $167.5 \pm 0.4$ MeV, with an energy resolution $\Delta E = 1.4$ MeV and a maximum intensity 0.1 μA. If the magnitude of the radial oscillations and, of course, the intensity, were reduced before extraction, the energy spread of beam was about $\Delta E = 0.5$ MeV, the

intensity decreasing to 10 nA on the target. Finally the complete experimental resolution was 0.85 MeV FWHM (see fig. 1).

The targets were set in the center of a scattering chamber, which was connected to a magnetic spectrometer. The scattered α-particles were counted by three scintillation telescopes located in the image plane of the magnet. Each telescope consisted of a small plastic scintillator (40 mm high, 6 mm large) in coincidence with a large scintillator situated behind. This last detector is used with a discriminator which eliminated the less ionizing particles. Control was made by a multichannel selector. The chosen targets were natural lead, tin, silicon and polystyrene or deuterated polyethylene. The two last targets allowed us to do some measurements on carbon but also on deuterium and hydrogen. Target thicknesses are shown in table 1.

TABLE 1

Thicknesses of the targets

| Nuclei | $(CH)_n$ | | $(CD_2)_n$ | | Si | Sn | Pb |
|---|---|---|---|---|---|---|---|
| | C | H | C | D | | | |
| Thickness (mg · cm$^{-2}$) | 29.1 | 2.4 | 20.0 | 6.6 | 218.4 | 160.5 | 115.1 |

The angular resolution was about 0.7°. It resulted from the angular aperture of the primary beam and of the spectrometer as well as from the width of the beam focused on the target. It would be very difficult to improve the angular resolution with the optics of the present synchrocyclotron. Absolute monitoring for this experiment was the greatest difficulty. We used a Faraday cup, a helium ionization chamber and a secondary electron chamber together. The cross sections were normalized on the inverse reaction $^4$He(p, p)$^4$He, interpolated between the results obtained at 39.8 MeV by Brussel *et al.* [6]) and at 55 MeV by Hayakawa *et al.* [7]). For elastic scattering the accuracy was limited by the monitoring. Absolute errors were about ±5 % for angles larger than 8°(lab) and ±10 % for smaller angles. Absolute errors for inelastic scattering may have been as great as ±15 % due to contamination from particles scattered by other levels.

## 3. Macroscopic analysis

### 3.1. ELASTIC SCATTERING

The elastic scattering of α-particles is described by an optical potential of Woods-Saxon shape

$$V_{\text{opt}} = V_C - V\left[1+\exp\left(\frac{r-r_R A^{\frac{1}{3}}}{a_R}\right)\right]^{-1} - iW\left[1+\exp\left(\frac{r-r_I A^{\frac{1}{3}}}{a_I}\right)\right]^{-1},$$

with six variable parameters. The Coulomb term $V_C$ corresponds to the potential produced by a uniformly charged sphere of radius $R_C = r_C A^{\frac{1}{3}}$. In this approximation the α-particle is considered as structureless although, in fact, its radius is not negli-

gible compared to the radii of some of the nuclei studied †. This would explain why the values of $r_R$ and $r_I$ are larger for light nuclei than for heavy nuclei.

The imaginary part of the optical potential is taken to be a volume term. The introduction of a surface term (first derivative of the Woods-Saxon well) did not appear to improve the fits. The automatic search on the six parameters was done using Perey's code JIB 3 [ref. [8])] adapted to our energy by increasing the number of partial waves. The accuracy of the fit is measured by

$$\chi_p^2 = \frac{1}{N}\sum_1^N \left[\frac{\frac{d\sigma}{d\Omega_{exp}} - \frac{d\sigma}{d\Omega_{th}}}{\Delta\left(\frac{d\sigma}{d\Omega_{exp}}\right)}\right]^2,$$

$N$ being the number of experimental points with error $\Delta(d\sigma/d\Omega_{exp})$.

TABLE 2

Optical-model parameters

| Nuclei | $V$ | $r_R$ | $a_R$ | $W$ | $r_I$ | $a_I$ | $r_C$ | $\chi_p^2$ |
|---|---|---|---|---|---|---|---|---|
| $^{12}C$ | 85.0 | 1.34 | 0.70 | 17.7 | 1.77 | 0.52 | 1.3 | 13.0 |
| | 100.9 | 1.21 | 0.76 | 14.7 | 1.86 | 0.48 | 1.3 | 10.0 |
| $^{28}Si$ | 109.7 | 1.25 | 0.81 | 24.6 | 1.63 | 0.51 | 1.4 | 2.2 |
| Sn | 127.6 | 1.19 | 0.88 | 22.0 | 1.50 | 0.60 | 1.5 | 5.2 |
| Pb | 118.0 | 1.25 | 0.71 | 23.1 | 1.39 | 0.81 | 1.5 | 16.1 |
| D WS | 32.4 | 1.73 | 0.59 | 67.4 | 0.93 | 0.43 | 1.4 | 5.8 |
| D G | 34.4 | 0.25 | 2.00 | 65.8 | 0.00 | 1.35 | 1.4 | 7.7 |

The classical value of $r_C$ is taken [42]) from the literature. Many tests show that the final result is not very sharply dependent on $r_C$. In table 2 the best parameters and the corresponding values of $\chi_p^2$ are given.

In the case of $^{12}C$ only, two different sets of parameters have been found; they are rather similar. We prefer the first set on the basis of a smooth dependence of parameters with mass number.

At small energies, there is an ambiguity in the determination of the optical potential [ref. [9])]. This ambiguity arises because, at low energies, the α-particle scattering is sensitive only to the tail of the potential, and this tail can be obtained from several alternative sets of potential parameters.

At 166 MeV, the α-particles penetrate further into the nucleus than at low energies. This permits a better determination of the optical potential. In fact the search was made for each nucleus varying (at the same time or not) $V$, $W$, $r_R$, $r_I$, $a_R$ and $a_I$ respectively between the values: 50-200, 10-50, 1.2-1.5, 1.0-1.9, 0.6-0.8, 0.4-0.8. The results obtained every time were quite similar. However, in some cases, the search converged to different results but with greater $\chi^2$ values and was considered thereby

† For $^{12}C$, $^{28}Si$, $^{208}Pb$ the rms radii are respectively 2.50 fm, 3.10 fm and 5.5 fm.

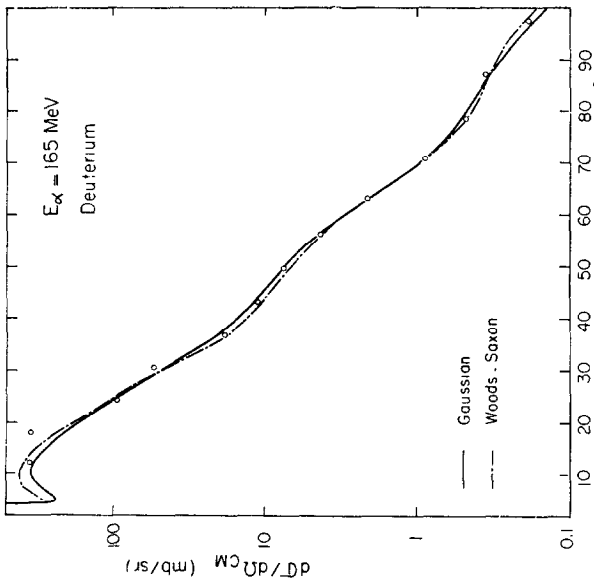


Fig. 3. Elastic scattering result for scattering on deuterium. Gaussian (solid line) and Woods-Saxon (dash and dot line) potentials.

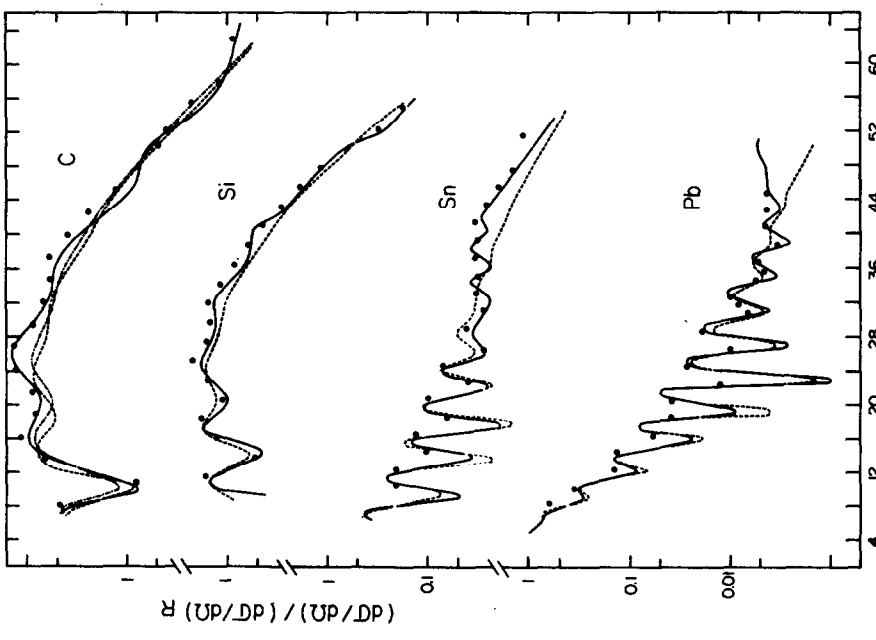


Fig. 2. Elastic scattering results. Experimental points and angular distributions with optical potentials: solid line - Woods-Saxon potential; dashed lines and dotted lines - calculated potential from nuclear matter density.

as not significant. Taking into account the only best $\chi^2$ results, we found a unique parameter set for each nucleus (except for carbon where two rather similar sets have been found).

We have made a similar search for the optical potential parameters from the results of Hauser *et al.* [4]). at 104 MeV. The determination is not unique but the ambiguity is much less than at low energies. For instance, in the case of the tin nucleus, three sets of parameters have been found (with the corresponding values of $V = 87.2$, 131.6 and 177.7 MeV). The $\chi^2_p$ results for the three sets are similar. One set is close to that obtained at 166 MeV.

A popular rule considers that the real optical potential for a projectile of $A$ nucleons of energy $E$ is $A$ times the potential of one nucleon having an energy $E/A$. For 40 MeV protons, the experiments show the real part $V$ equals 39 MeV implying that the real potential for 80 MeV deuterons or for 160 MeV $\alpha$-particles should be respectively 78 MeV and 156 MeV. The experimental values are respectively about 70 MeV [ref. [10])] and 120 MeV. This discrepancy may be due to the neglection of the binding energy of d and $\alpha$-particles and multiple scattering. The real part of the optical potentials for 120 MeV tritons or helium 3 can then be deduced by interpolation between the preceding value corresponding to 80 MeV deuterons and 160 MeV $\alpha$-particles. By application of the rule quoted before, one sees that the value should be about 95 MeV.

In fig. 2 the experimental elastic cross section and the theoretical curves calculated from the potentials from table 2 are presented. Fig. 3 shows the experimental results for deuterium.

With regard to the potential parameters found, we make the following remarks:

– many tests show that, if the experimental differential cross sections are modified by $\pm 10\,\%$, the parameters remain about the same;

– the parameters of the potential obtained from this experiment are very close, principally for carbon, silicon and tin;

– in the case of lead the theoretical curves are rapidly oscillating. The experimental dips are partially filled due to the angular resolution. This fact could explain the high value of $a_I$ [see the systematic tests of Rolland [11])];

– a comparison of the results of this experiment with those of the elastic scattering of 155 MeV protons [11]) shows that the values of the potential radii for $\alpha$-particle scattering are larger than those for proton scattering; this point is explained partially by the size of $\alpha$-particles;

– the diffuseness of the real potential for protons and $\alpha$-particles (about 0.75 fm) at 160 MeV is larger than the diffuseness obtained for $\alpha$-particles at smaller energies. For $\alpha$-particles, as for protons, the imaginary radius is larger than the real radius. The scattering of $\alpha$-particles at low energies [12]) gives a larger radius and smaller diffuseness; the absorption of $\alpha$-particles increases when their energy decreases and the nucleus seems more like a black disk;

– if we compare with other results we see that the potentials, obtained by Duhm [3])

at 119 MeV for magnesium, are very similar to ours although they obtained several alternative sets of values. Our analysis of the experimental results of Hauser *et al.* [4]) at 104 MeV gives several sets of potentials, one of which corresponds to the one obtained at 166 MeV;

– the use of diffraction models in our conditions is of little interest because it can only explain the position of minima and maxima and its validity is certainly suspect for light nuclei. This is because the nuclei do not appear to be black disks for 166 MeV α-particles. Further, this model defines values of diffraction radii clearly lower (about 1.5 fm for tin) than those obtained with 40 MeV α-particles by Fernandez [13]) or by Yavin *et al* [14]). The results of Hauser *et al.* [4]) at 104 MeV, treated in this way, give values slightly larger than ours. These results confirm, at least qualitatively, the preceding remarks.

– for deuterium the elastic scattering was analysed with two different complex potentials one having a Gaussian shape and the other a Woods-Saxon shape. The corresponding results are presented in table 2; these two potentials are in fact very similar and give values of $\chi_p^2$ close enough to correspond to a single solution.

### 3.2. INELASTIC SCATTERING

Differential cross sections were measured for the levels $2^+$ (4.43 MeV), $3^-$ (9.64 MeV), $0^+$ (7.66 MeV) of $^{12}C$, $2^+$ (1.78 MeV) of $^{28}Si$ and $2^+$ of Sn. The first $2^+$ level for each abundant isotope of Sn is very close to 1.2 MeV.

We find that the phase rule is almost respected at small angles. The $0^+$ state of carbon expected, these levels can be described by phenomenological rotational or vibrational models which makes possible their analysis by the DWBA formalism of Bassel *et al.* [15]). In this formalism the interaction producing the nuclear excitation is described as the first derivative of the real and imaginary parts of the optical potential $V_{opt}$ as determined by elastic scattering. The corresponding form factor is

$$\frac{i^l \beta_l R}{a\sqrt{2l+1}} \frac{\mathrm{d}V_{opt}}{\mathrm{d}r},$$

where $\beta_l$ is the deformation parameter of the level excited by the transfer of angular momentum $l$; $\beta_l$ is, for a rotational model, the permanent deformation and, for a vibrational model, the mean deformation corresponding to nuclear surface oscillations. The computations were made by DWUCK [16]), adapted to the energy conditions of this experiment. Fig. 3 shows the theoretical and experimental angular distributions; in table 3 the $\beta_l$ values obtained by us and by other inelastic scattering experiments are given.

From fig. 4 and table 3 one ascertains a good agreement for the angular distribution both in shape and absolute value, for tin, which has a very small $\beta_l$. For the other nuclei the deformation is larger and the agreement between theoretical and experimental cross sections is less good, but the form of the theoretical angular distribution

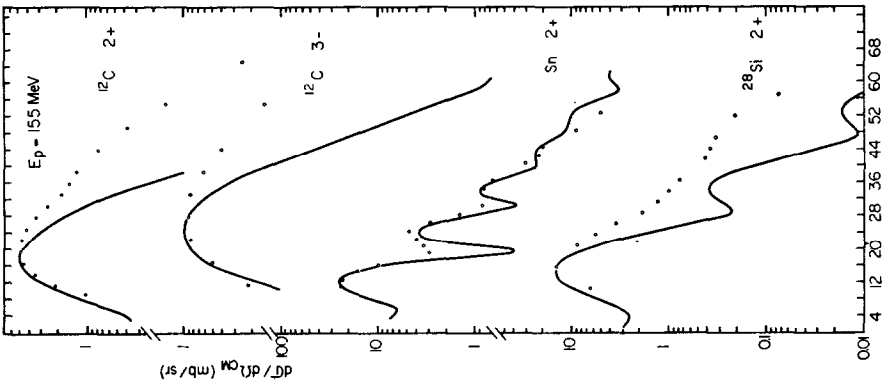


Fig. 5. Inelastic scattering results for the same levels excited by 155 MeV protons. The curves correspond to the following values of $\beta_2$ = 0.59 for $^{12}$C, 0.32 for $^{28}$Si, 0.138 for Sn and of $\beta_3$ = 0.38 for $^{12}$C.

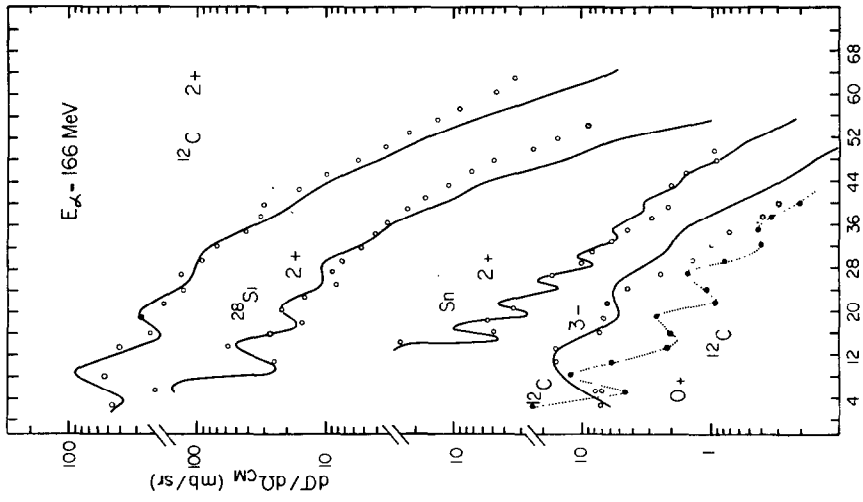


Fig. 4. Inelastic scattering results. Curves obtained from phenomenological macroscopic model (with $\beta_l$ values pointed out in table 3).

TABLE 3

$\beta_l$ deformation parameters deduced from this experiment. Comparison with other results

| This experiment | | | Other analysis | | |
|---|---|---|---|---|---|
| | | $\beta_l$ | $\beta_l$ | projectiles | Ref. |
| | | | 0.59 . . . 0.90 | protons | [20,26,17,18] |
| | $2^+$ | 0.30 | 0.38 | alpha | [21,18] |
| | | | 0.30 | heavy ions | [19,23,22] |
| $^{12}C$ | | | 0.37 | | |
| | | | 0.38 | protons | [17] |
| | $3^-$ | 0.18 | 0.57 | | [26] |
| | | | 0.44 | | [24] |
| | | | 0.32 | protons | [17,18] |
| | | | 0.25 | | [26] |
| $^{28}Si$ | $2^+$ | 0.24 | 0.4 | | [27] |
| | | | 0.3 | | |
| | | | 0.22 | alpha | [25] |
| | | | 0.138 | protons | [17] |
| Sn | $2^+$ | 0.10 | 0.09 | alpha | [30] |

is satisfactory. This is not always true for other projectiles; see fig. 5. for instance, for 155 MeV protons [17]).

For the $2^+$ excited level of carbon values of $\beta_2$ were obtained varying from 0.3 to 0.9 depending on the method of analysis (DWBA, Blair . . .) for the same experimental results, on the shape (at low energy) of the imaginary potential (surface, volume) and on the nature of the projectile (p, d, $^3$He, α, heavy ions), their energy, etc.

It is possible, also, to analyse the results of this experiment in terms of the reduced probability for electromagnetic transitions.

For the quadrupolar transition we have the relation

$$B(\mathrm{E2}, 2^+ \rightarrow 0^+) = \frac{1}{5}\left[\frac{3ZeR_0^2\beta_2}{4\pi}\right]^2,$$

calculated for a spheroidal nucleus, with deformation parameter $\beta_2$, mean radius $R_0$ and a uniform distribution of charge on its surface. [For the experimental value of $B$(E2) see ref. [29]) and specially for tin see ref. [30]).] For tin, again, our result agrees with that obtained from Coulomb excitation or electron scattering; but the agreement is not good for the other nuclei, silicon perhaps excepted. Comparison with the theoretical values [30]) shows that the calculations of Lombard and Campi-Benet [28]) are the most satisfactory for tin. On the other hand, several new theoretical results of Lamme *et al.* [31]) are close to ours for carbon and silicon. Our result, for carbon, is lower than the value calculated from the hole-particle wave functions of Gillet and Vinh-Mau [32]) and from the Hartree-Fock wave functions of Bouten *et al.* [33]).

## 4. Microscopic analysis

### 4.1. AN EFFECTIVE αN INTERACTION

Assuming a Gaussian shape for the form factor of the NN interaction, Glendenning and Veneroni [34]) have derived an αN effective interaction of the form

$$V(\bar{r}, \bar{r}_\alpha) = V_0 \exp(-|\bar{r}-\bar{r}_\alpha|^2/\mu^2).$$

They proposed the parameter values $V_0 = -34$ MeV and $\mu = 2.26$ fm. More recently Bernstein [35]) gave the slightly different values $V_0 = -37$ MeV and $\mu = 2$ fm. The last parameter seems to be rather well defined [36]). Jackson [37]) has considered variations of the range $\mu$ between 1.77 fm and 2.3 fm and in a recent work [38]) has also chosen $\mu = 2$ fm. Consequently we have fixed $\mu = 2$ fm and not tried to vary it systematically.

The above effective interaction was calculated for a zero-energy αN scattering. It is reasonable to introduce a renormalization parameter $u_R$ and search for its best value by fitting theoretical to experimental cross sections. The new effective αN interaction

$$V_{\text{eff}} = V(\bar{r}, \bar{r}_\alpha)u_R$$

is then energy dependent through the parameter $u_R$.

### 4.2. THE OPTICAL POTENTIAL FOR ELASTIC αN SCATTERING

4.2.1. *The fundamental formula.* Jackson [37,38]) has proposed to compute the real part of the α-nucleus potential by the formula

$$V^R_{\text{opt}} = \int V_{\text{eff}}(\bar{r}, \bar{r}_\alpha)\rho(\bar{r})\mathrm{d}\bar{r},$$

where $\rho(\bar{r})$ is the nuclear matter distribution. We will consider only spherical nuclei. The isotropic radial density $\rho(r)$ is normalized by

$$\int \rho(r)r^2\,\mathrm{d}r = A/4\pi,$$

$A$ being the number of nucleons in the target. For our interaction, the real part of the optical potential is given by

$$V^R_{\text{opt}}(r) = u_R V_0 \frac{2\pi\mu^2}{r_\alpha}\int \rho(r)\exp[-(r^2+r_\alpha^2)/\mu^2]\sinh\left(\frac{2rr_\alpha}{\mu^2}\right) r\,\mathrm{d}r.$$

To obtain reasonable fits we need, of course, a complex potential. We make the assumption [35,36]) that the imaginary part is proportional to the real part:

$$V^I_{\text{opt}}(r) = i\frac{u_I}{u_R}V^R_{\text{opt}}(r),$$

where $u_I$ is a new parameter to be fixed, as $u_R$, by a $\chi_p^2$ search. Thus our optical potential will read:

$$V_{opt}(r) = V_{opt}^{R}(r) + V_{opt}^{I}(r) = (u_R + iu_I)\int V(\bar{r}, \bar{r}_\alpha)\rho(\bar{r})d\bar{r}.$$

4.2.2. *Variation of $u_R$ and $u_I$ with $V(\bar{r}, \bar{r}_\alpha)$.* In table 4 we show the best values of $u_R$ and $u_I$ determined for $^{208}$Pb for the effective interaction of Glendenning and Veneroni, and of Bernstein. The nuclear matter distribution is one obtained in a Hartree-Fock calculation by Vautherin and Veneroni [39]). The $\chi^2$ values are those obtained by

TABLE 4

Values of the parameters $u_R$ and $u_I$, and of $\chi_p^2$ for the effective interactions of Glendenning and Veneroni, and of Bernstein

| Force | $V_0$ (MeV) | $\mu$ (fm) | $u_R$ | $u_I$ | $\chi_p^2$ | Remarks |
|---|---|---|---|---|---|---|
| 1 | −37 | 2 | 1 | 0 | $2.4 \cdot 10^8$ | real part only, without search |
| | | | 1 | 0.64 | 96 | search on the imaginary part only |
| | | | 0.61 | 0.33 | 24 | |
| 2 | −34 | 2.26 | 0.41 | 0.19 | 32 | |

TABLE 5

Variation of the parameters $u_R$ and $u_I$ with nuclear matter densities for Pb nucleus

| Density | Ref. | $u_R$ | $u_I$ | $\chi_p^2$ |
|---|---|---|---|---|
| HF | [39]) | 0.61 | 0.33 | 24 |
| Fermi | [35]) | 0.72 | 0.39 | 24 |
| NSW | [41]) | 0.79 | 0.44 | 24 |

TABLE 6

Variation of the parameters $u_R$ and $u_I$ with nuclear matter densities for Sn, Si and C nuclei

| Target | Density | Ref. | $u_R$ | $u_I$ | $\chi_p^2$ |
|---|---|---|---|---|---|
| Sn | HF | [40]) | 0.69 | 0.36 | 32.5 |
| | Fermi | [35]) | 0.75 | 0.39 | 29 |
| $^{28}$Si | Fermi | [35]) | 0.66 | 0.27 | 13.8 |
| $^{12}$C | shell-model harmonic oscillator | [42]) | 0.71 | 0.32 | 24 |
| | HF | [40]) | 0.89 | 0.41 | 62.5 |

minimizing the difference between experiment and "microscopic" theory. The large value of $\chi^2$ in line 1 simply emphasize that the imaginary part of the optical potential cannot be neglected. In line two we see that including $u_I$ gives drastically improvement but in order to obtain a fit as good as was obtained with a Woods-Saxon shape poten-

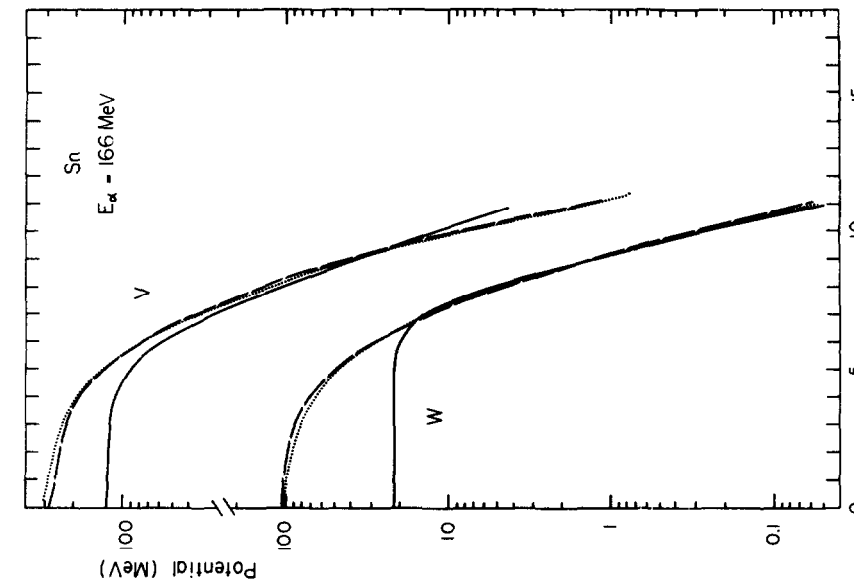


Fig. 7. Optical potentials: solid line - WS; dashed line - Fermi; dotted line - HF.

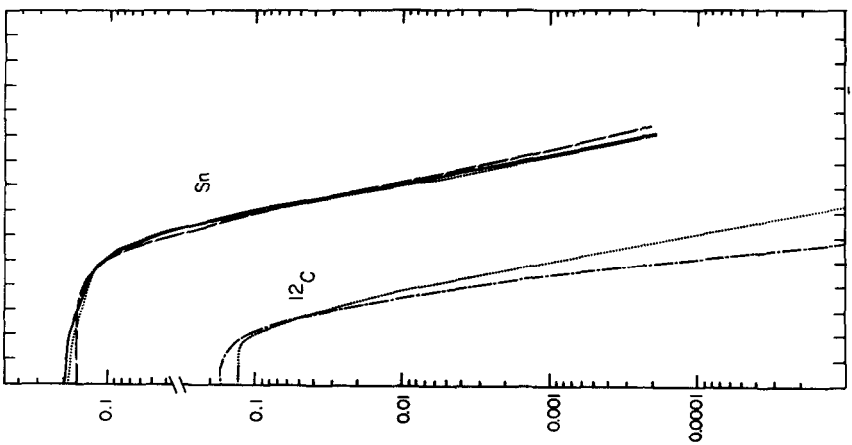


Fig. 6. Nuclear matter density: dotted line - HF; (solid line - HF also for another tin isotope); dashed line - Fermi; dot and dash line - shell model.

tial ($\chi^2_{WS} \approx 16$) one has to treat $u_R$ as adjustable, as in lines 3 and 4. We find $u_R/u_I$ is nearly two for both interactions. Changing the range of $\mu$ by 10 % has doubled $u_R$ and $u_I$. In the remainder of our calculations we choose interaction 1.

TABLE 7

$\chi_p^2$ values corresponding to the average parameters $\bar{u}_R$ and $\bar{u}_I$

| Target | Density | Ref. | $\bar{u}_R$ | $\bar{u}_I$ | $\chi_p^2$ | $\chi_{p\,ws}^2$ |
|---|---|---|---|---|---|---|
| Pb | HF | [39]) | 0.7 | 0.35 | 85 | 16.1 |
| | HF | [40]) | 0.7 | 0.35 | 76 | |
| | Fermi | [35]) | 0.7 | 0.35 | 54 | |
| Sn | HF | [40]) | 0.7 | 0.35 | 37 | 5.2 |
| | Fermi | [35]) | 0.7 | 0.35 | 34 | |
| $^{28}$Si | Fermi | [35]) | 0.7 | 0.35 | 53 | 2.2 |
| $^{12}$C | HF | [40]) | 0.7 | 0.35 | 164.5 | 13 |
| | shell model | [42]) | 0.7 | 0.35 | 46 | |

TABLE 8

Values of the parameters $u_R$ and $u_I$ at different energies

| Target | $E_{lab}$ (MeV) | Density | Ref. | $u_R$ | $u_I$ | $\chi_p^2$ |
|---|---|---|---|---|---|---|
| Pb | 166 | HF | [39]) | 0.61 | 0.33 | 24 |
| Sn | 166 | HF | [40]) | 0.69 | 0.36 | 32.5 |
| $^{28}$Si | 166 | Fermi | [35]) | 0.66 | 0.27 | 13.8 |
| $^{12}$C | 166 | shell model | [42]) | 0.71 | 0.32 | 24.0 |
| $^{12}$C | 166 | HF | [40]) | 0.89 | 0.41 | 62.5 |
| $^{208}$Pb | 104 | HF | [40]) | 0.71 | 0.57 | 25.8 |
| $^{124}$Sn | 104 | HF | [40]) | 0.78 | 0.55 | 17.7 |
| $^{40}$Ar | 104 | Fermi | [35]) | 0.75 | 0.40 | 87.8 |
| $^{16}$O | 104 | shell model | [42]) | 0.78 | 0.26 | 45.3 |
| $^{12}$C | 104 | shell model | [42]) | 0.82 | 0.31 | 13.3 |
| $^{58}$Ni | 64.3 | Fermi | [35]) | 0.79 | 0.31 | 296 |
| $^{208}$Pb | 44 | HF | [40]) | 0.92 | 1.32 | 334 |
| $^{124}$Sn | 44 | HF | [40]) | 0.87 | 0.33 | 388 |
| $^{120}$Sn | 44 | HF | [40]) | 0.72 | 0.29 | 212 |
| $^{58}$Ni | 44 | Fermi | [35]) | 0.64 | 0.44 | 1350 |
| $^{40}$Ca | 44 | Fermi | [35]) | 0.80 | 0.22 | 824 |
| $^{24}$Mg | 44 | Fermi | [35]) | 0.70 | 0.30 | 548 |
| $^{12}$C | 104 | shell model | [42]) | 0.85 | 0.32 | 11.8 |
| $^{208}$Pb | 44 | HF | [40]) | 1.15 | 2.26 | 570 |

4.2.3. *Variation of $u_R$ and $u_I$ with the nuclear matter density for different nuclei.* The results for the lead nucleus are presented in table 5. We will compare the agreement given by several matter distributions. The Fermi distribution $\rho = \rho_0[1+\exp((r-c)/0.57)]^{-1}$ with $c = 6.495$ fm, is that proposed by Bernstein for nuclei from $^{20}$Ne to $^{206}$Nb in table 7 of ref. [35]). The density noted N.S.W. [41]) is a three parameters

Fermi function proposed for the neutron distribution of $^{208}$Pb, where $\omega = 0.40$, $c_p = c_{n=p} = 6.30$ fm. The last parameter $c_{ne} = 6.56$ fm corresponds to the neutron excess.

It appears from table 5 that the theoretical densities give parameter values, similar to those obtained from phenomenological densities. It also appears that the $\chi^2_p$ value is quite satisfactory compared to the value given by the Woods-Saxon optical potential ($\chi^2_{p\,WS} = 16.1$).

The results for the tin and silicon nuclei are presented in table 6 and figs. 2, 6 and 7. Several results are given for different matter densities and in each case, $u_R$, $u_I$ and $\chi^2_p$ corresponding to the best fit. Only results obtained from the Hartree-Fock [40]) matter distribution have been plotted on fig. 2 for lead and tin nuclei, the curves corresponding to Fermi distributions being quite similar.

The oscillator shell-model density [42]) for the carbon nucleus having the form

$$\rho = \rho_0(1+\alpha r^2/a_0^2)\exp\left[-(r/a_0)^2\right],$$

with $a_0 = 1.635$ fm and $\alpha = \frac{4}{3}$, gives a good $\chi^2_p$ result. Note that, although the target nucleus is not large compared to an α-particle, we can use the same effective interaction. On the contrary, our result is bad using a HF spherical density. The discrepancy is then probably due to the deformation of $^{12}$C. For the shell-model density, the harmonic oscillator parameter was obtained from elastic electron scattering results; in this way the deformation was probably averaged. One can see in fig. 6 the difference between the two densities. The curves corresponding to the carbon nucleus are drawn in fig. 2, dotted line – shell-model density; dash and dot line – HF density.

The values obtained for the two variable parameters can be averaged over all the preceding results. We then obtain $\bar{u}_R = 0.7$ and $\bar{u}_I = 0.35$. Using these values the calculations were repeated, the optical potential being now calculated without an adjustable parameter. The results are given in table 7. The value of $\chi^2_p$ obtained using the average parameters are compared with $\chi^2_{p\,WS}$ resulting from the phenomenological search with a Woods-Saxon potential containing six adjustable parameters.

### 4.3. VARIATION WITH α-PARTICLE ENERGY

The results of an analysis of some α-particle elastic scattering differential cross sections at 104 MeV [ref. [4])], 64.3 MeV [ref. [2])] and 44 MeV [ref. [43])] are given in table 8. The mean value of $\chi^2_p$ is greater at 44 MeV (and 64.3 MeV) because of the smaller errors at these energies (from 1 % to 2 %). The dispersion found for $u_R$ and $u_I$ increases as the α-particle energy decreases. Notice that the value $u_R/u_I \approx 0.5$ is greater than the corresponding ratio $W/V$ of the Woods-Saxon potential. This may be explained by the fact that, in the microscopic calculation, we have chosen the same geometry for the real and imaginary terms, while in the Woods-Saxon case, the automatic research gave $R_I > R_R$. The shape of the potentials is, however, similar at the nuclear surface.

The preceding calculations have been done taking into account all the experimental results independently of the angle. However it is possible that the cross sections at large angles strongly depend on the terms describing transitions through intermediate excited states [36]). The results obtained for $u_R$ and $u_I$ would then be falsified by the fitting process including experimental results at large angles. One could think that such an effect should be important in $^{12}C$ where the first collective $2^+$ level is strongly excited. The calculations have been repeated for 104 MeV α-particles scattered by $^{12}C$, taking only into account experimental results up to 45° c.m. (compared to 105° c.m. before). The result is given at the bottom of table 8; one can see that agreement is not improved.

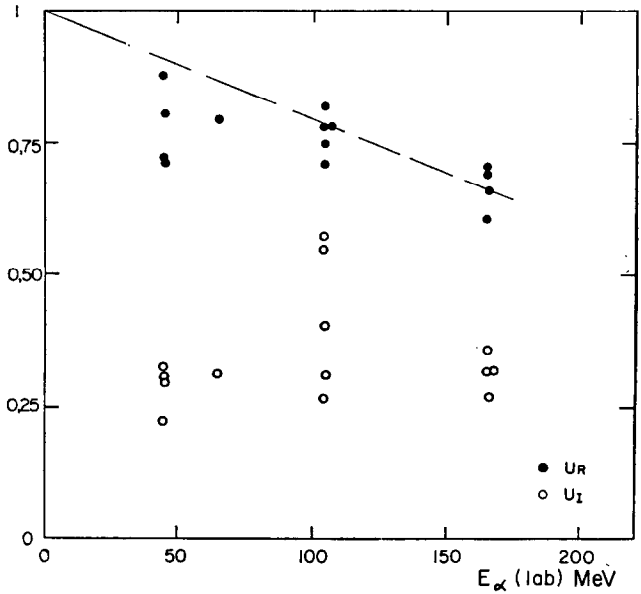


Fig. 8. Values of $u_R$ and $u_I$ obtained at different energies for different targets.

At 44 MeV, the results for Pb and Ni are not plotted in fig. 8 because they are far from the averaged values. It seems that the search with only two adjustable parameters becomes less useful at that lower energy. For instance one sees at the bottom of table 8 that the result for $^{208}Pb$, obtained using only half of the experimental points, those at angles smaller than 67°4, is very different.

Finally if as in fig. 8 we consider only results obtained at 166 MeV and 104 MeV, the extrapolation of $u_R$ is compatible with the value 1 for zero energy justifying partly the treatment of the αN interaction.

### 4.4. INELASTIC SCATTERING

Having now determined an αN interaction, it is possible to study the wave functions of inelastically excited levels by means of DWBA calculations. Some of the difficulties

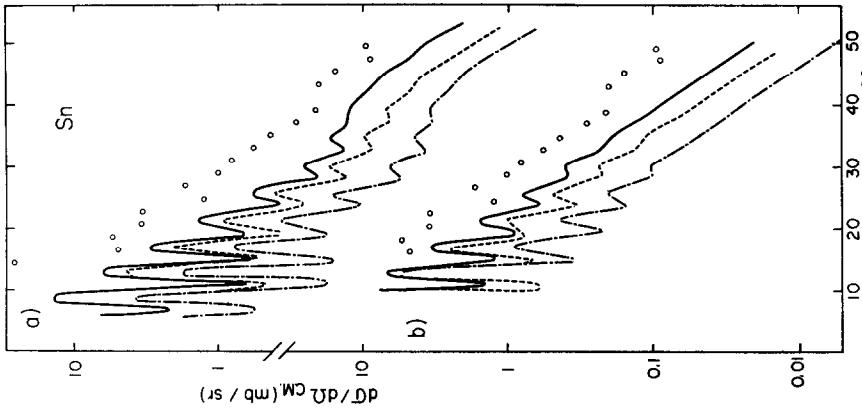


Fig. 10. Differential cross sections for the $2^+$ level of $^{120}Sn$. The different curves correspond to the Clement and Baranger's model (solid line), Gillet's model (dashed line), model of Arvieu *et al.* (dot and dash line), the part a corresponding to the macroscopic optical potential and the part b to the microscopic optical potential.

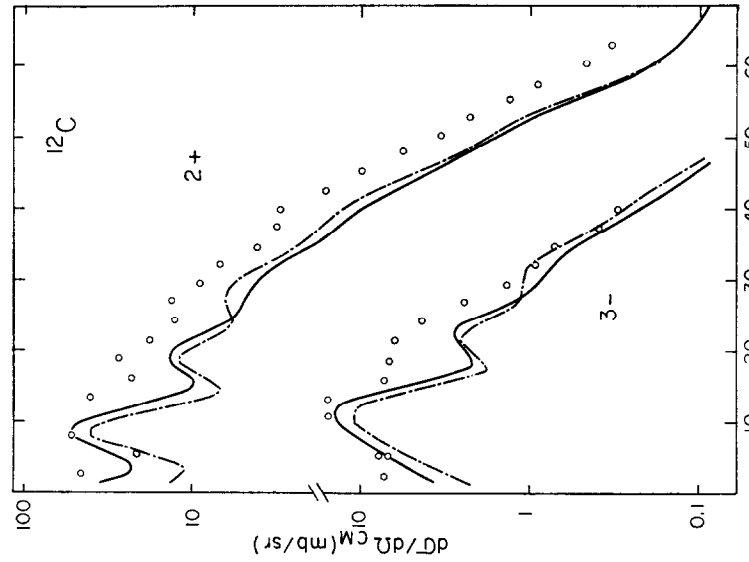


Fig. 9. Differential cross sections for $2^+$ and $3^-$ levels of $^{12}C$. The optical potentials used in the calculations have been obtained by the macroscopic (dashed line) or microscopic (solid line) method.

such as the antisymmetry [44]) which exists in the proton case seem less important for α-particles.

The interaction is also simpler because there are no spin or isospin exchange terms.

We use the effective αN interaction determined above, and a nuclear matter distribution which gives good optical potentials in the entrance and exit channels. We also use the same effective interaction for the calculation of form factors. We use hole-particle or quasiparticle wave functions. We then obtain inelastic cross sections through a completely microscopic calculation without any new adjustable parameter.

The scattering amplitude

$$T_{\mathrm{if}}^{M_\mathrm{f}} = \int \mathrm{d}\bar{r}\, \chi_\mathrm{f}^{-*}(\bar{k}_\mathrm{f}, \bar{r}) \langle \mathrm{f}|V_{\mathrm{eff}}|\mathrm{i}\rangle \chi_\mathrm{i}^{+}(\bar{k}_\mathrm{i}, \bar{r})$$

gives the differential cross sections [15])

$$\frac{\mathrm{d}\sigma}{\mathrm{d}\Omega} = \frac{\mu}{2\pi\hbar^2}\,\frac{k_\mathrm{f}}{k_\mathrm{i}} \sum_{M_\mathrm{f}} |T_{\mathrm{if}}^{M_\mathrm{f}}|^2. \qquad (J_\mathrm{i} = 0)$$

The nuclear wave functions are of the following types: $|\mathrm{i}\rangle = |0\rangle$

$$|\mathrm{f}\rangle = \sum_{Ab} \chi_{Ab}(-1)^{j_b+\frac{1}{2}} \sum_{\substack{m_A m_b \\ t_{zA} t_{zb}}} (-1)^{j_b - m_b} \langle j_A\, m_A\, j_b - m_b | J_\mathrm{f}\, M_\mathrm{f}\rangle \times (-1)^{\frac{1}{2}-t_{zb}} \langle \tfrac{1}{2} t_{zA}\, \tfrac{1}{2} - t_{zb} | T_\mathrm{f}\, 0\rangle a_{mA}^{+} a_{mb} |0\rangle,$$

where $a_{mA}^{+}$ and $a_{mb}$ are the usual creation and annihilation operators.

Using Messiah's [45]) notation, we obtain

$$\langle \mathrm{f}|V_{\mathrm{eff}}|\mathrm{i}\rangle = (-1)^L 2\sqrt{2\pi} V_0 (u_\mathrm{R} + i u_\mathrm{I}) \sum_{Ab} R_{Ab}\, \chi_{Ab}\, \hat{j}_A\, \hat{j}_b\, \hat{l}_A\, \hat{l}_b \times \begin{pmatrix} l_A & l_b & L \\ 0 & 0 & 0 \end{pmatrix} \begin{Bmatrix} l_b & l_A & L \\ j_A & j_b & \frac{1}{2} \end{Bmatrix} \sum_{m=-L}^{+L} Y_L^m(\Omega r_\alpha),$$

$$\hat{j}_A = (2j_A + 1)^{\frac{1}{2}},$$

$$R_{Ab} = \int u_A(r_\alpha) u_b(r_\alpha) \exp\left[-(r^2 + r_\alpha^2)/\mu^2\right] J_L(2irr_\alpha/\mu^2) r_\alpha^2 \mathrm{d}r_\alpha,$$

where $R_{Ab}$ is expressible in terms of confluent hypergeometric functions if the $u(r)$ are harmonic oscillator wave functions.

4.4.1. *The carbon nucleus.* We used the particle-hole wave functions obtained by Gillet and Vinh-Mau [32]) in the RPA approximation. The value of the harmonic oscillator parameter is 1.64 fm. Comparison between theory and experiment is given in fig. 9 for the $2^+$ and $3^-$ states. There are no great differences between the curves obtained from the macroscopic and microscopic optical potentials. The fit with experiment is rather good for these wave functions which do not take account of the carbon deformation.

4.4.2. *The tin nucleus.* Several wave functions exist for the $2^+$ states of tin isotopes. All describe the levels as quasiparticle neutron configurations, but proton configurations are not always taken into account. For the harmonic oscillator

parameter, in each case, we have taken the value used in the model calculation.

The results† for $^{120}$Sn are plotted in fig. 10. The dotted and dashed curves correspond to the model of Arvieu *et al.* [46])††. There, only neutron configurations act coherently, and the calculated values are too small by a factor 13. The dashed curves

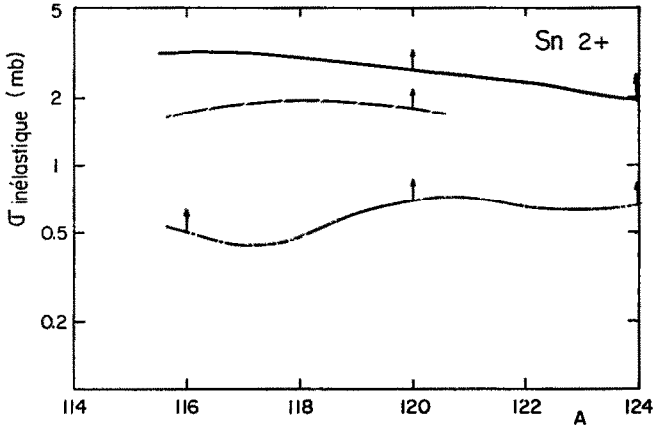


Fig. 11. Total inelastic cross section for the $2^+$ level of several tin isotopes. Some conventions as in fig. 10 have been chosen for the three curves. The optical potential is issued from macroscopic calculations, the arrows indicate what occurs when microscopic optical potentials is used.

correspond to results obtained with Gillet's [47]) wave functions. There, neutron and proton configurations act coherently. Nevertheless the results remain too small by a factor 6.5. However the form of the differential cross sections remains the same whatever the number of configurations or their coherency are. We can apply the procedure proposed by Schaeffer [44]) who introduced two parameters $\lambda_p$ and $\lambda_n$ renormalizing the proton and the neutron configurations. With this values: $\lambda_p = 7$ and $\lambda_n = 1.4$, we obtain an enhancement of 6.4 which is in remarkable agreement with the factor 6.5 given before. The full curves correspond to the calculations done with wave functions of Clement and Baranger [48]). They have included a greater number of configurations (33) which all act coherently. The theoretical differential cross sections are still too small, but by a factor of 3.5 only. Taking the value $\lambda_p = 2.4$ deduced from the ratio of experimental to calculated values [48]) of $B$(E2), we obtain $\lambda_n = 1.65$. Although these numbers are not very precise, it seems that the proton configurations are less well described than neutron configurations.

In fig. 10 the upper part a corresponds to calculations using the macroscopic optical potential, and the lower part b, to the microscopic optical potential already described for which $\bar{u}_R = 0.7$ and $\bar{u}_I = 0.35$. The microscopic potential seems to give better

† We thank V. Comparat for his help for matrix elements calculations with quasiparticle wave functions.

†† There is a misprint in table 8 a of ref. [46]). It concerns the 116 and 124 Sn isotopes.

results in so far as the normalizing ratio is more constant for different scattering angles and the oscillations are reduced.

The experimental points correspond to a natural tin target, the $A = 120$ isotopes being the most important. The variation of theoretical results from one isotope to another, is given by fig. 11 where we have plotted the total inelastic cross section for the $2^+$ level. For other isotopes, the situation is similar but favouring still more the wave functions of Clement and Baranger. The arrow indicates the enhancement of the total cross section obtained when the calculation is done with the microscopic optical potential (as in b). If we assume that the ratio between experimental and theoretical values remains approximately constant with angle, the experimental total inelastic cross section would be 10 mb.

## 5. Conclusion

We have presented, here, results of 166 MeV α-particles elastically and inelastically scattered by some nuclei. At that energy the incident particles penetrate more deeply into the nucleus than at lower energies. In consequence the macroscopic optical potential is better determined. That determination allows us to obtain deformation parameters from inelastic scattering results with better accuracy. In spite of the good agreement between experimental and theoretical angular distributions the values of deformation parameters are different from the values obtained with incident protons.

From the analysis of our experimental results, we have obtained an effective αN interaction, which is almost the same for different nuclei at different energies. This method allows the discussion of nuclear matter distributions. We found that HF matter distributions are good for Sn and Pb but not for $^{12}C$. However it appears that the method used does not allow a distinction between different matter distributions if they are not very different from each other; or, in other words, it is not very sensitive. On the other hand, our analysis is interesting because of the very small number of free parameters. Using our αN potential, we were able to get reasonable agreement with the elastic and the inelastic differential cross sections of several authors at a number of energies. Such a coherent description of a large body of experimental data is encouraging.

Because we introduce no free parameter in our discussion of the inelastic scattering we can attempt to determine the excited state wave functions. For $^{12}C$ a particle-hole wave function description was rather successful; for Sn the results were not as good.

We would like to acknowledge the cordial help of Professor M.K. Brussel. Thanks are also due to Dr. M. Sowinski for his cooperation in experimental work. We are extremely indebted to Professor M. Veneroni for many encouraging discussions during the course of this work. We thank him, Dr. D. Vautherin and Dr. X. Campi-Benet for communication of unpublished HF results. We are very grateful to Professor N. Marty for her continued interest for this work, to Dr. A. Bernstein for many critical discussions, and to Professor D. Sprung for his help for the writing of the manuscript.

## References


1) C. R. Bingham, M. L. Halbert and R. H. Bassel, Phys. Rev. **148** (1966) 1174
2) P. Darriulat *et al.*, report UCRL 11054
3) H. H. Duhm, Nucl. Phys. **A118** (1968) 563
4) G. Hauser *et al.*, Nucl. Phys. **A128** (1969) 81; report KFK 871
5) I. Brissaud, M. K. Brussel, M. Sowinski and B. Tatischeff, Phys. Lett. **30B** (1969) 324
6) M. K. Brussel and J. H. Williams, Phys. Rev. **106** (1957) 286
7) S. Hayakawa *et al.* Phys. Lett. **8** (1964) 330
8) F. Perey (ORNL), private communication
9) L. MacFadden and G. R. Satchler, Nucl. Phys. **84** (1966) 177
10) G. Duhamel, Doctorat de spécialité (1969) Orsay
11) C. Rolland, thesis Orsay (1966);
    C. Rolland, B. Geoffrion, N. Marty, M. Morlet, B. Tatischeff and A. Willis, Nucl. Phys. **80** (1966) 625
12) G. R. Satchler, Nucl. Phys. **70** (1965) 177
13) B. Fernandez, thesis University of Paris (1969)
14) A. S. Yavin and G. W. Farwell, Nucl. Phys. **12** (1959) 1
15) R. H. Bassel *et al.*, Phys. Rev. **128** (1962) 2693
16) C. Kunz, University of Colorado, unpublished
17) V. Comparat, B. Geoffrion, N. Marty, M. Morlet, C. Rolland, B. Tatischeff and A. Willis, private communication
18) T. Stowall and N. M. Hintz, Phys. Rev. **B135** (1964) 330
19) J. C. Hiebert and G. T. Harvey, Phys. Rev. **B135** (1964) 346
20) G. R. Satchler, Nucl. Phys. **A100** (1967) 481
21) E. Rost, Doctoral dissertation, University of Pittsburgh (1961)
22) R. H. Bassel *et al.*, Nucl. Phys. **89** (1966) 419
23) R. H. Bassel *et al.*, Azilomar Conf. (1963) 45
24) M. P. Fricke and G. R. Satchler, Phys. Rev., to be published
25) J. Korame *et al.*, J. Phys. Soc. Jap. **20** (1965) 475
26) R. M. Haybron, Nucl. Phys. **79** (1966) 33
27) P. H. Stelson *et al.*, to be published
28) R. J. Lombard and X. Campi-Benet, Nucl. Phys. **83** (1966) 303
29) P. H. Stelson and L. Grodzins, Nucl. Data **A1** (1965) 21
30) G. Bruge *et al.*, Nucl. Phys. **A146** (1970) 597
31) H. A. Lamme and E. Bocker, Nucl. Phys. **A136** (1969) 609
32) V. Gillet and N. Vinh-Mau, Nucl. Phys. **54** (1964) 321
33) M. Bouten and P. van Leuven, Ann. of Phys. **43** (1967) 421
34) N. K. Glendenning and M. Veneroni, Phys. Rev. **144** (1966) 839
35) A. M. Bernstein, Advances in nuclear physics, eds. M. Baranger and E. Vogt (1970) vol. 3, p. 325
36) A. M. Bernstein, private communication
37) D. F. Jackson, Phys. Lett. **14** (1964) 118
38) C. G. Morgan and D. F. Jackson, Phys. Rev. **188** (1969) 1758
39) D. Vautherin and M. Veneroni, Phys. Lett. **29B** (1969) 203
40) X. Campi-Benet, private communication
41) J. A. Nolen Jr., J. P. Schiffer and N. Williams, Phys. Lett. **27B** (1968) 1
42) R. Hofstadter, Nuclear and nucleon structure (W. A. Benjamin, New York, 1963)
43) G. Bruge, Internal CEA Report R 3147
44) C. Schaeffer, thesis Orsay (1969) internal CEA report R4000
45) A. Messiah, Quantum mechanics (North-Holland, 1961 and Dunod, 1959)
46) R. Arvieu, thesis, Orsay (1963); Ann. de Phys. **8** (1963) 407;
    R. Arvieu, E. Baranger, M. Veneroni, M. Baranger and V. Gillet, Phys. Lett. **4** (1963) 119
47) V. Gillet and B. Giraud, private communication
    V. Gillet, B. Giraud and H. Rho, Phys. Rev. **178** (1969) 1695
48) D. M. Clement and E. Baranger, Nucl. Phys. **A120** (1968) 25
    T. T. S. Kuo, E. Baranger and M. Baranger, Nucl. Phys. **81** (1966) 241